

# Frequency-Selective MHz Power Amplifier for Dielectric Barrier Discharge Plasma Generation

JIALE XU <sup>1</sup> (Member, IEEE), KAWIN SURAKITBOVORN <sup>1</sup> (Student Member, IEEE), BENJAMIN WANG<sup>2</sup>,  
MARK A. CAPPELLI <sup>2</sup>, AND JUAN RIVAS-DAVILA <sup>1</sup> (Senior Member, IEEE)

<sup>1</sup>Department of Electrical Engineering, Stanford University, Stanford, CA 94305 USA

<sup>2</sup>Department of Mechanical Engineering, Stanford University, Stanford, CA 94305 USA

CORRESPONDING AUTHOR: JIALE XU (e-mail: jialexu@stanford.edu)

**ABSTRACT** Plasma-assisted nitrogen fixation at atmospheric pressure is a clean and decentralized method for fertilizer production. Among many different plasma discharge types, dielectric barrier discharge (DBD) is one of the few that can generate high output of nitrogen compounds at atmospheric conditions for fertilizer usage. Most DBD generators operate at kHz switching frequencies, however, previous research has found that discharge activities occur at the intervals of the greatest voltage slew rate. The finding implies that operating at higher frequencies can lead to more discharge activities and higher plasma generation. This paper presents a MHz Class E power amplifier with frequency selection to generate DBD plasma at two distinct frequencies. The power amplifier achieves a peak efficiency of 91.5% and outputs 600 W at frequencies of 12.4 MHz and 15.5 MHz.

**INDEX TERMS** Resonant power conversion, Plasma applications, Power amplifiers.

## I. INTRODUCTION

The Haber-Bosch process is one of the most impactful chemical reactions in history. This process improves agricultural yield by increasing ammonia fertilizer production, helping in feeding the world's growing population. In 2020, global ammonia production was around 144 million metric tons [1], and more than 95% of ammonia is produced through the Haber-Bosch process [2]. Between 75% to 90% of the ammonia produced is used in making fertilizer, benefiting 50% of the world's food production [3]. The Haber-Bosch process fixes nitrogen with hydrogen to produce ammonia with the feedstock of natural gas (50%), oil (31%) or coal (19%) [2]. Burning these fossil fuels during the process leads to more than 1% of the world's total CO<sub>2</sub> emission. The process requires a centralized plant for high-temperature and high-pressure reactions. After the production, the ammonia then needs to be transported to local farms. The transportation not only has environmental and cost concerns, it is also dangerous since ammonia is highly toxic and flammable when exposed to high temperatures [4].

Recently, Non-Thermal Atmospheric Pressure Plasma (NTAPP) has gained attention as a sustainable replacement for conventional nitrogen fixation process [5]. With the development of low-temperature plasma science, the minimum theoretical energy consumption of non-thermal plasma-assisted fixation is lower than that of the Haber-Bosch process [6]. The fixation process applies plasma at the surface of air and water to form soluble reactive oxygen and nitrogen species (RONS). The species include nitrate (NO<sub>3</sub><sup>-</sup>) and other forms of nitrogen compounds, which can all be used as fertilizers [5], [7]. Plasma-assisted nitrogen fixation works under atmospheric conditions without emission of green house gases. Localized production due to the reduced system size and simplified process also eliminates potential cost and hazards during transportation.

The literature has discussed different discharge types for nitrogen fixation, including microwave plasma, spark discharge, gliding arc discharge, and dielectric barrier discharge (DBD) [6]. Among these alternatives, both the gliding arc discharge and DBD have high output of NO<sub>x</sub> compounds and can

operate under atmospheric pressure. This work focuses on designing a power amplifier to produce DBD plasma. Most DBD systems use power supplies that generate a low-frequency (in the range of 50 Hz to a few tens of kHz) multi-kV output at the plasma load [8]. Previous research has shown that the discharge activities occur during the zero crossings of the applied voltage, corresponding to the intervals of the greatest voltage slew rate and maximum current [9]. The finding implies that increasing the frequency can lead to more discharge activities and higher plasma production rate, motivating the design of a MHz power amplifier to drive a DBD plasma load.

Conventionally, RF system manufacturers use linear power amplifiers in high-frequency applications, including plasma generation. The linear power amplifiers have the advantages of linearity but low efficiencies. The switch-mode power amplifiers such as Class D, Class E, and Class  $\Phi_2$  can achieve much higher efficiencies under zero-voltage-switching (ZVS) operations. However, due to their resonant nature, these switch-mode power amplifiers maintain high efficiencies only at a fixed frequency and constant load condition. Previous research has introduced different methods to extend the frequency and load range, including reactance compensation [10], impedance compression [11], phase-switched impedance modulation [12], and load-independent power amplifier design [13]. The power delivered to a plasma load at MHz can be much higher than that at kHz due to higher plasma generation rate. As a result, it is necessary to operate the power amplifier at a low burst rate to reduce the average power delivered to the DBD reactor. This paper presents a wideband Class E power amplifier using the reactance compensation technique and combined with frequency selection networks to drive multiple DBD loads sequentially. The frequency selection networks allow the power amplifier to operate for longer time within each burst period while each DBD reactor only receives a fraction of the total average power.

One challenge before designing the power amplifier is to measure the plasma load impedance. Before the plasma breakdown, the load is almost entirely reactive. To start the plasma, one requirement is to carefully tune the matching network to minimize the reflective power. After the plasma breakdown, the load has an additional resistive part, and the resistance varies significantly with the operating conditions. Depending on the reactor design and operating conditions, the plasma load after the breakdown can still be very reactive, making it hard to measure precisely. Section II describes the DBD electrode design and plasma impedance measurement in details. The rest of the paper is organized as follows. Section III explains the design of the frequency-selective power amplifier; Section IV shows the experimental results; and Section V concludes the paper.

## II. ELECTRODE DESIGN AND PLASMA LOAD MEASUREMENT

A DBD reactor has two electrodes located on the opposite sides of a dielectric barrier [8]. The electrode on the front side is exposed to air, and the electrode on the back side is covered

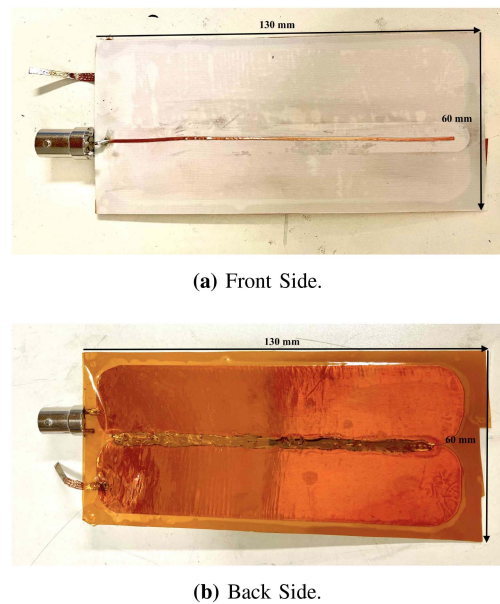


**FIGURE 1.** The (a) front side and (b) back side of the designed DBD reactor using 0.2 mm Rogers 4003 C dielectric board.

by a layer of dielectric material. Generating DBD plasma at MHz frequencies requires a careful selection of the dielectric material for the board to produce a certain capacitance with low loss. Previous research has used mica at 13.56 MHz [14]. In this work, Rogers 4003C [15] is used because of its low dissipation factor at high frequencies and the possibility of it being integrated into a PCB to keep the costs low. Figure 1(a) shows the electrode on the front side of the Rogers board made by a thin line of copper tape, and Figure 1(b) shows the grounded electrode on the back made by a copper plane covered by a layer of Kapton tape. After experimenting with several different widths of the front electrode and thicknesses of the Rogers board, the designs with low capacitance (narrow copper lines on the front side) and small board thickness are found to break down at lower voltages. The electrodes used in this work has a board thickness of 0.2 mm, a front electrode width of 1 mm, and a length of 100 mm. The plasma strikes when the voltage across the electrodes of this DBD reactor exceeds  $700 V_{rms}$ . After the plasma strikes, a plasma sheath forms only around the top electrode without a breakdown of the dielectric. The detailed measurement procedure will be described later in this section.

Plasma load impedances are sensitive to the operating conditions, such as temperature, pressure, and power delivered [9]. Before the plasma generation starts, the load is nearly purely reactive; after the plasma breakdown, the load impedance changes with the increased applied voltage, especially for the resistive part. A commercial linear power amplifier is used to drive the plasma load for impedance measurement. When the power amplifier drives a highly reactive load, most of the power gets reflected, which makes it hard to reach the voltage for plasma breakdown. Therefore,

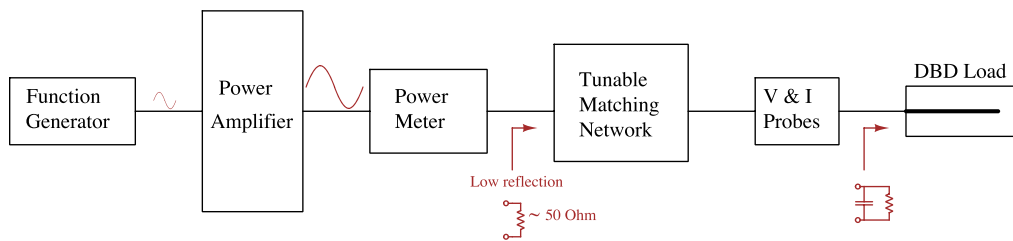


**FIGURE 2.** The setup for measuring the impedance of a DBD plasma load.

it is necessary to match the plasma load to  $50 \Omega$  using a tunable matching network and actively adjust the network as the plasma impedance changes. Calibration of the probes is also essential for accurate measurements, especially the phase angle between the voltage and current. Even after the breakdown, the plasma load can still have a relatively high quality factor (Q), and a small skew can result in a large error in the measured impedance. Knowing the caveats above, the measurement of the load impedance in a DBD plasma system includes the following steps:

#### 1) VOLTAGE AND CURRENT PROBE CALIBRATION

The voltage measurement requires a capacitor divider by connecting a high-voltage COG capacitor between the load and the probe because of the high breakdown voltage of the plasma load. The current probe used in the measurement setup is Pearson current monitor 2878. Before connecting to the DBD load, it is important to calibrate the probes. The calibration includes measuring the voltage and current across a  $50 \Omega$  radio-frequency (RF) load driven by a linear power amplifier (ENI A1000) at the desired frequency and power level. During this measurement, it is important to adjust the skew time between the two probes to make the phase angle between them  $0^\circ$ . The measured  $\frac{V_r}{I_r}$  is a reference for  $50 \Omega$ .

#### 2) SMALL SIGNAL IMPEDANCE MATCHING OF THE DBD LOAD TO $50 \Omega$

After calibrating the probes, the next step is to connect them to the DBD load and measure the small signal impedance with a tunable matching network connected to the load. The tunable matching network can be adjusted until the measured impedance is  $50 \Omega$ . Taking the measurements with the probes connected allows for better matching, since the capacitance of the DBD load can be small (on the order of a few pF to hundreds of pF depending on the electrode design). The small signal measurement sets the initial matching conditions before the system is powered on, which accelerates the impedance matching in the next step.

#### 3) MEASUREMENT OF THE DBD PLASMA LOAD

The DBD load and the matching network are then connected to the linear power amplifier and a power meter (Keysight N1914 A). Figure 2 illustrates the overall measurement setup. Figure 3 shows the setup of the voltage and current probes

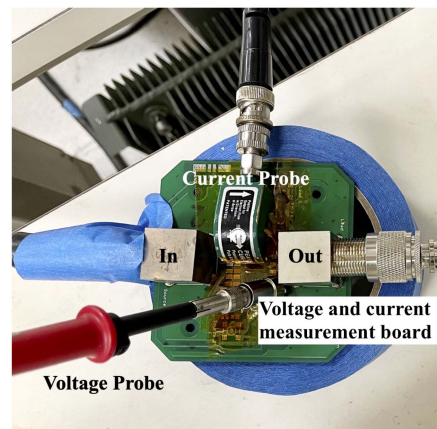


**FIGURE 3.** Setup of the voltage and current probes (V & I Probes) in Figure 2. The voltage measurement uses a capacitor divider. The current measurement uses the Pearson current monitor 2878. The input terminal connects to the tunable matching network, and the output terminal connects to the DBD load.

(V & I Probes) in Figure 2. The voltage probe connects to a capacitor divider to measure the high output voltage. The Pearson current monitor 2878 is used to measure the current. The input terminal connects to the tunable matching network, and the output terminal connects to the DBD load. As the applied voltage increases, the matching network can be adjusted when the reflected power becomes significant. Finally at the desired output power after the plasma breakdown, the voltage and current measurements are taken along with the phase angle between them ( $V_m$ ,  $I_m$ ).

#### 4) CALCULATE THE PLASMA LOAD IMPEDANCE

Using the  $\frac{V_r}{I_r}$  reference for  $50 \Omega$  in step 1) and the voltage and current measurements in step 3), the following equation calculates the plasma impedance:

$$Z_{load,plasma} = \frac{V_m}{I_m} \times \frac{V_r}{I_r} \times 50 \quad (1)$$

Figure 4 shows the measured plasma impedance at 13.56 MHz in terms of the parallel resistance and capacitance as modeled in Figure 5. The plasma breakdown starts at an input power of around 200 W and an output voltage of  $700 V_{rms}$ . As the power increases after the breakdown, the output voltage stays relatively unchanged, but the length of

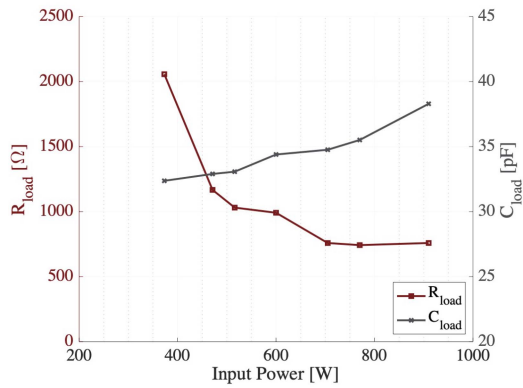


**FIGURE 4.** The measured plasma impedance at different input power at 13.56 MHz in terms of the parallel resistance and capacitance. The measured output voltage is 700  $V_{rms}$  and stays relatively unchanged after the plasma strikes at 200 W.

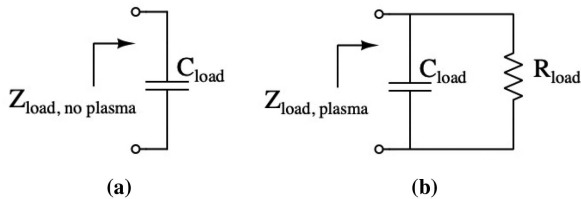


**FIGURE 5.** Schematics of the equivalent load impedance (a) before the plasma breakdown, (b) after the plasma breakdown.

the plasma strip generated at the front electrode gradually extends, causing a decrease in the resistance. The plasma strip reaches the full length of the front electrode at about 600 W. The measured load impedance has a parallel capacitance of 33 pF (including 13 pF of the connectors and the board) and a resistance of 758  $\Omega$  with a phase angle of approximately  $-70^\circ$ . Because of its significant real part, the measured impedance provides a relatively reasonable estimate of the plasma load impedance. However, depending on the plasma type, electrode design, and the operating conditions, the load impedance can have a close-to- $\pm 90^\circ$  phase angle. In those cases, it can be challenging to measure the plasma impedance accurately using voltage and current probes. In step 4), it is also possible to use the input power and output voltage measurements to calculate the plasma impedance. However, the input power measurement includes the power lost in the matching network, which can make the impedance measurement less accurate.

### III. DESIGN OF THE FREQUENCY-SELECTIVE POWER AMPLIFIER

Most of the DBD plasma generators operate at low switching frequencies. However, [9] has shown that most of the discharge activities occur during the intervals of the greatest voltage slew rate and maximum current, implying a higher plasma generation rate at a higher frequency. As the frequency increases into MHz, the amount of the plasma generated can result in a much higher power delivery to the load. Even with the high-frequency dielectric materials, it is still hard for the

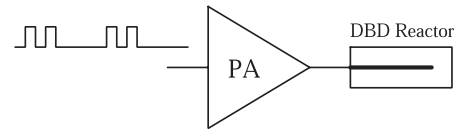


**FIGURE 6.** Illustration of the power amplifier driving one DBD reactor at a low burst rate.

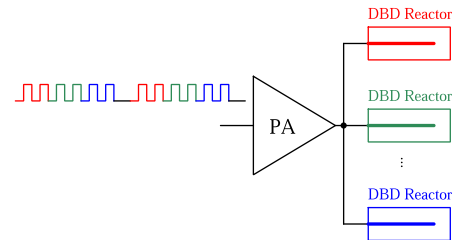


**FIGURE 7.** Illustration of the power amplifier driving multiple DBD reactors in a sequential manner.

DBD reactor to dissipate all the power. Therefore, the need to operate the power amplifier at a low burst rate arises to avoid such high power dissipation in the load, as illustrated in Figure 6. However, operating at a low burst rate is not a good utilization of the power amplifier’s high power delivering capability. A better operation of the power amplifier is to drive multiple loads sequentially. As illustrated in Figure 7, within each pulsing period, the power amplifier is delivering power selectively to only one of the DBD reactors, which is labeled by the same color as the input signal. As a result, the power amplifier is able to operate longer, while each DBD reactor only receives a fraction of the total average power. The literature has introduced a few techniques for selective power delivery, including using switch selection [16], and frequency selection [17]. Both techniques require active switches to either selectively connect to the load or be used in the switched capacitor banks to change the resonant frequency.

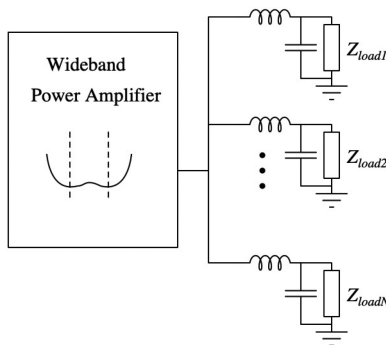
Depending on the applications, these switches may require high voltage blocking and fast switching capabilities, as well as auxiliary gate drive circuitry, which could be complicated for the non-ground-referenced switches. In contrast, this paper proposes to use the similar idea of frequency selection but without any additional switches. Table 1 compares the selective power delivery technique presented in this work with the two mentioned above. Using only passive elements makes the design less expensive and less complicated. Similar to the frequency selection technique using switched capacitor banks, the design presented in this work also requires a wide bandwidth so that selective power delivery can be achieved by setting different switching frequencies.

Figure 8 shows the proposed frequency-selective power delivery system. The LC resonant networks connecting to the loads are resonating at different frequencies, and all of these resonant frequencies are within the bandwidth of the designed wideband power amplifier. The prototype design of a frequency-selective Class E power amplifier to drive two DBD loads follows the design procedure below.



**TABLE 1. Comparison of the Selective Power Delivery Technique Presented in This Work With Those in Previous Publications**

	[16]	[17]	This Work
<i>Selection Technique</i>	Switch selection	Frequency selection	Frequency selection
<i>Additional Switches</i>	Yes	Yes	No
<i>Circuit Implementation</i>	Active switches	Switched capacitor banks with active switches	LC networks resonating at different frequencies
<i>Bandwidth Limitation</i>	N/A	Wideband	Wideband



**FIGURE 8. Frequency-selective power delivery by using a wideband power amplifier to drive multiple loads.**

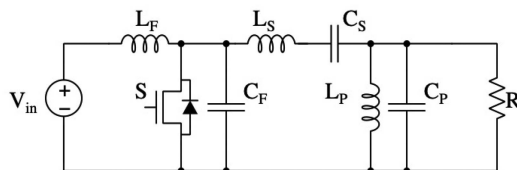


**FIGURE 9. Schematic of the load-independent Class E power amplifier.**

1) DESIGN THE CLASS E POWER AMPLIFIER

Figure 9 shows the Class E power amplifier with finite DC-feed inductance that is able to maintain efficient ZVS operations when driving a variable load [13].

$L_F$  and  $C_F$  are the main design components to meet ZVS, while the output network of  $L_S$ - $C_S$ - $L_P$ - $C_P$  filters out higher harmonics. Following the design steps in [13],  $L_F$  and  $C_F$  can be calculated:

$$\frac{1}{\sqrt{L_F C_F}} = 2\pi f_{IN},$$

$$\sqrt{\frac{L_F}{C_F}} = k_f R_{min}, \tag{2}$$

where  $f_{IN} = 1.4 \times f_S$  ( $f_S$  is the switching frequency, 13.56 MHz in this case) and  $k_f = 1$ . The input voltage is 200 V and the power is 600 W based on the measurements from Figure 4.

2) EXTEND THE BANDWIDTH OF THE POWER AMPLIFIER

The conventional switch-mode power amplifiers only operate at a single frequency. When shifting away from the designed

frequency, both the efficiency and output power degrade significantly. Extending the bandwidth for the frequency-selective power amplifier is necessary to ensure efficient operations at different frequencies and same power delivery to all of the loads. The literature proposes different methods to extend the bandwidth of these power amplifiers, including tunable and switchable matching networks and reactance compensation techniques [10], [18], [19], [20], [21]. This work uses reactance compensation because it only requires two sets of LC resonant tanks ( $L_S$ - $C_S$  and  $L_P$ - $C_P$ ), which are already in the design. The first step is to design  $L_S$  and  $C_S$  based on the output filtering requirement and the targeted bandwidth. A larger  $Q_S$  makes the output more sinusoidal with less harmonics but the trade-off is a smaller bandwidth. In this design,  $Q_S$  is selected to be 2.5 to provide a bandwidth that covers the targeted operating frequencies. Next,  $L_P$  and  $C_P$  are calculated based on the reactance compensation requirement following the equations below: [22]

$$C_F + \frac{1}{\omega^2 L_F} = \frac{2}{\omega R} (Q_S - Q_P),$$

$$\frac{1}{\sqrt{L_P C_P}} = \omega,$$

$$\frac{1}{\sqrt{L_S C_S}} = \omega, \tag{3}$$

where  $Q_P = \omega R C_P$ ,  $Q_S = \frac{\omega L_S}{R}$ ,  $\omega$  is the the center frequency, and  $R$  is the output resistance of the Class E power amplifier determined in the previous step. Substituting the  $C_F$  and  $L_F$  calculated from the previous step,  $Q_S = 2.5$ , and  $\omega = (2\pi)13.56$  MHz into the equation results in a  $Q_P$  of 1.48.

3) DESIGN THE OUTPUT RESONANT NETWORKS FOR THE TWO LOADS

Selective power delivery to one of the two loads requires two output resonant networks, resonating at different frequencies. Figure 10 shows the schematic of the output networks.

The first design requirement is to deliver the same amount of power to the active plasma load at the corresponding frequency. Specifically,

$$\frac{V_1}{V_{out}} \text{ at } f_1 = \frac{V_2}{V_{out}} \text{ at } f_2, \tag{4}$$

which leads to

$$Q_1 = Q_2, \tag{5}$$

where  $Q_1 = 2\pi f_1 (C_1 + C_{load}) R_{load}$ ,

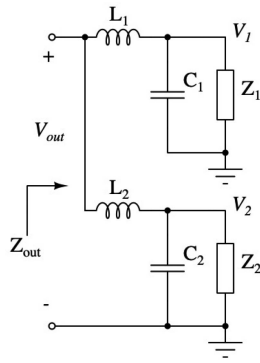


**FIGURE 10.** Schematic of the output resonant networks in the design.  $Z_1$  and  $Z_2$  are the DBD loads as modeled in Figure 5, where only one of them at a time generates plasma.

$$Q_2 = 2\pi f_2(C_2 + C_{load})R_{load},$$

$$\text{and } f_1 = \frac{1}{2\pi \sqrt{L_1(C_1 + C_{load})}},$$

$$f_2 = \frac{1}{2\pi \sqrt{L_2(C_2 + C_{load})}}, \quad (6)$$

where  $f_1$  is the operating frequency to deliver power to the plasma load  $Z_1$ ,  $f_2$  is the frequency to deliver power to  $Z_2$ , and  $C_{load}$  and  $R_{load}$  are defined in Figure 5. At  $f_1$ ,

$$Z_1 = R_{load} // \frac{1}{2\pi f_1 C_{load}},$$

$$Z_2 = \frac{1}{2\pi f_1 C_{load}}, \quad (7)$$

and at  $f_2$ ,

$$Z_1 = \frac{1}{2\pi f_2 C_{load}},$$

$$Z_2 = R_{load} // \frac{1}{2\pi f_2 C_{load}} \quad (8)$$

The second requirement is to make the voltage across the active plasma load to be significantly larger than the other load voltage:

$$V_1 \gg V_2 \text{ at } f_1,$$

$$V_2 \gg V_1 \text{ at } f_2, \quad (9)$$

so that only one load at a time is receiving power and generating plasma. Designing for a minimum voltage ratio of 2 ( $\frac{V_1}{V_2} > 2$  at  $f_1$ , and  $\frac{V_2}{V_1} > 2$  at  $f_2$ ) requires

$$\left|1 - \left(\frac{f_1}{f_2}\right)^2\right| |Q_1| > 2,$$

$$\left|1 - \left(\frac{f_2}{f_1}\right)^2\right| |Q_2| > 2 \quad (10)$$

A high  $Q$  allows the two designed frequencies to be close together; however, it also makes the network hard to tune and sensitive to component variations, including the variation in

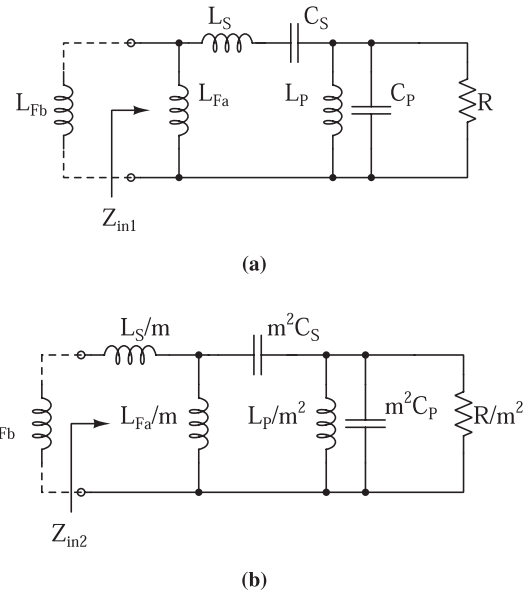


**FIGURE 11.** Impedance transformation of the designed Class E power amplifier's output network. The input impedances of the two networks ( $Z_{in1}$  and  $Z_{in2}$ ) are equal.

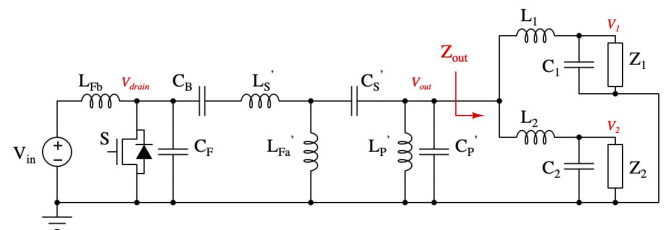


**FIGURE 12.** Overall schematic of the design.

the plasma capacitance. A low  $Q$  requires the two frequencies to be farther apart, but at the same time, both  $f_1$  and  $f_2$  need to be within the bandwidth of the designed power amplifier. For a plasma load of  $C_{load} = 20$  pF and  $R_{load} = 758 \Omega$ ,  $Q = 5$  is selected for both output networks with  $f_1 = 12$  MHz and  $f_2 = 15.5$  MHz.

The third requirement is to make sure the output impedance ( $Z_{out}$ ) at  $f_1$  and  $f_2$  are equal. If  $Z_{out}$  at the two frequencies are not the same due to the interaction of the two close resonances, additional tuning of the component values as well as the designed frequencies can help to achieve equal  $Z_{out}$ .

**4) MATCH THE OUTPUT RESISTANCE TO THE PLASMA LOAD**  
The last step is to match the output resistance of the designed Class E power amplifier to the total impedance of the load ( $Z_{out}$ ). Figure 11 shows the impedance transformation of the power amplifier's output resistance by a factor of  $\frac{1}{m^2}$  using Norton transform [23], [24], where

$$m = \frac{L_S}{L_{Fa}} + 1 \quad (11)$$

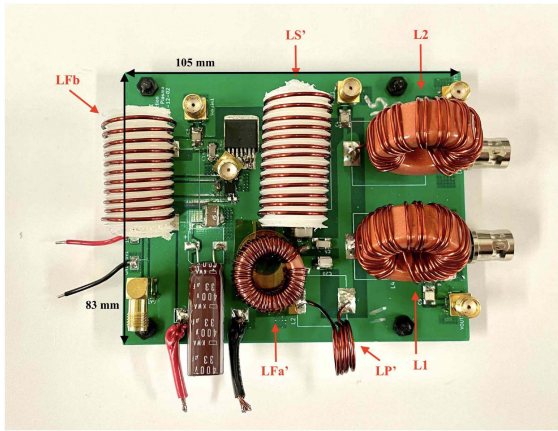


FIGURE 13. PCB of the frequency-selective Class E power amplifier.

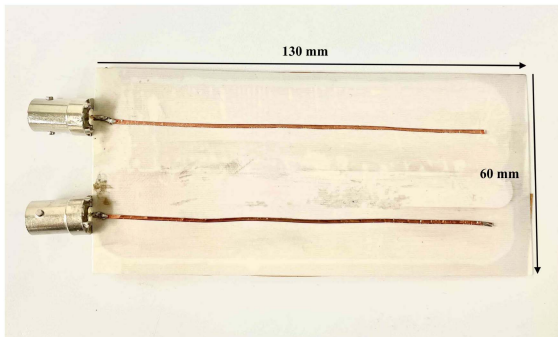


FIGURE 14. Front side of the electrode design including two DBD loads.

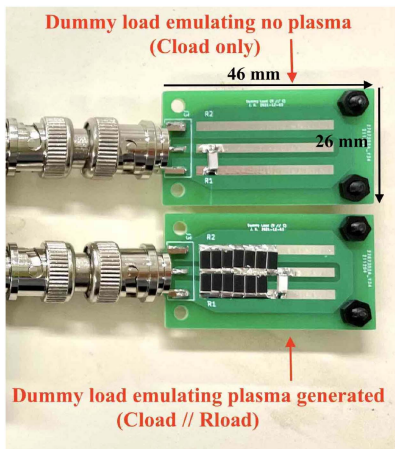


FIGURE 15. The dummy loads designed using high-voltage resistors and capacitors to emulate the DBD loads with and without plasma generated.

and  $L_{Fa}$  is part of  $L_F$  in Figure 9, where

$$L_F = L_{Fa} // L_{Fb} \tag{12}$$

The reactive part of  $Z_{out}$  can be combined to  $L_P$  or  $C_P$ , so that

$$\text{Re}(Z_{out}) = \frac{R}{m^2} \tag{13}$$

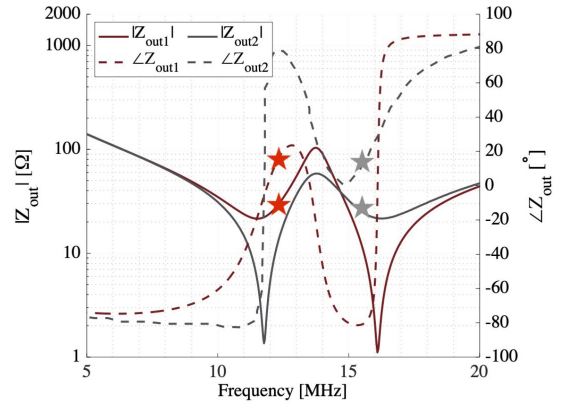


FIGURE 16. Measured small signal output impedances ( $Z_{out}$ ).  $Z_{out}$  at  $f_1 = 12.4$  MHz (labeled with red stars) roughly equals  $Z_{out}$  at  $f_2 = 15.5$  MHz (labeled with grey stars).

TABLE 2. Design Parameters of the Frequency-Selective Class E Power Amplifier

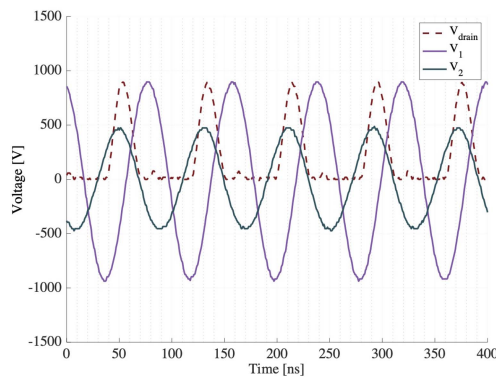
Parameter	Value
$V_{in}$	200 V
$P$	600 W
$f_1$	12.4 MHz
$f_2$	15.5 MHz
$S$	G3R350MT12J
$L_{Fb}$	1.12 $\mu$ H
$C_B$	4 nF
$C_F$	68 pF
$L_{S'}$	1.35 $\mu$ H
$L_{Fa'}$	1.54 $\mu$ H
$C_{S'}$	200 pF
$L_{P'}$	225 nH
$C_{P'}$	690 pF
$L_1$	1.83 $\mu$ H
$C_1$	79 pF
$L_2$	1.36 $\mu$ H
$C_2$	52 pF
$C_{load}$	20 pF
$R_{load}$	758 $\Omega$

One of the advantages of this technique is that the impedance waveform across frequency is exactly the same after the transformation. Therefore, the transformation step does not change the bandwidth of the designed power amplifier. Figure 12 shows the overall schematic of the design, and Table 2 lists the design parameters.

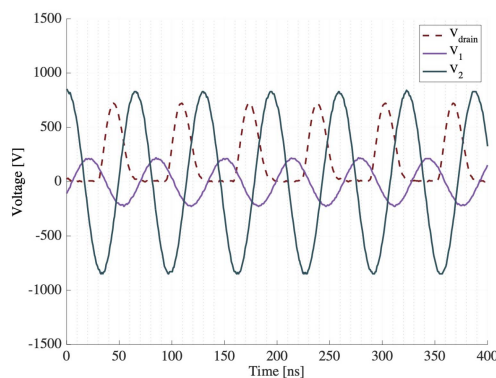
#### IV. EXPERIMENTAL RESULTS

This section discusses the experimental results of the design presented, including the small-signal impedance, power, and efficiency measurements.

First, it is necessary to measure the small-signal output impedances ( $Z_{out}$ ) of the designed power amplifier (Figure 13)



(a) 12.4 MHz.



(b) 15.5 MHz

**FIGURE 17.** Measured waveforms of  $V_1$ ,  $V_2$ , and  $V_{drain}$  (output voltages across the two loads and the drain voltage of the switch) at (a) 12.4 MHz and (b) 15.5 MHz.

at  $f_1$  and  $f_2$  to ensure that they match at the two frequencies. Figure 14 shows the modified front side of the electrode design to include two DBD loads, where each top electrode has the same dimensions as the one in Figure 1(a). Figure 15 shows the dummy loads to measure the impedance and efficiency. The dummy loads are designed using high-voltage resistors and capacitors to emulate the DBD loads with and without plasma generated. The measured output impedances shown in Figure 16 confirm that  $Z_{out}$  at  $f_1 = 12.4$  MHz roughly equals  $Z_{out}$  at  $f_2 = 15.5$  MHz.

The next step is to test the design with the dummy loads and calculate the system efficiency using the voltage measurements  $V_1$  and  $V_2$  and the dummy load resistance. Figure 17 shows the waveforms of  $V_1$ ,  $V_2$ , and  $V_{drain}$  at 12.4 MHz and 15.5 MHz. The drain voltage waveforms show ZVS switching behaviors at the two frequencies.  $V_1$  at  $f_1 = 12.4$  MHz and  $V_2$  at  $f_2 = 15.5$  MHz are significantly larger than the voltage across the no-plasma load in each case, ensuring the power delivery and plasma generation only at the selected load. The ratios of  $\frac{V_1}{V_2}$  at  $f_1$  and  $\frac{V_2}{V_1}$  at  $f_2$  are not the same, because otherwise,

$$2\pi f_1 L_2 = 2\pi f_2 L_1, \quad (14)$$

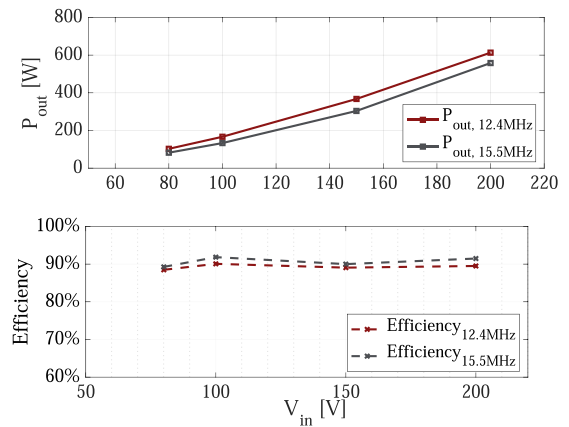


**FIGURE 18.** Measured output power and efficiency of the design driving the dummy loads at 12.4 MHz (in red) and 15.5 MHz (in gray). The output power is calculated based on the measured output voltage and the equivalent parallel resistance of the dummy loads.

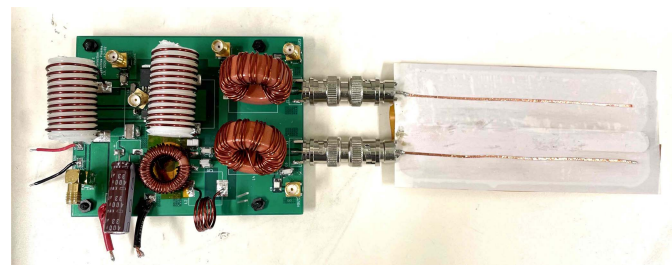


**FIGURE 19.** The frequency-selected Class E power amplifier driving the DBD loads.

which contradicts Equation 5 for  $f_1 \neq f_2$ . Ensuring the same power delivery to each load is more critical than keeping  $\frac{V_1}{V_2}$  at  $f_1$  and  $\frac{V_2}{V_1}$  at  $f_2$  equal as long as the voltages across the no-plasma loads are much lower than the plasma breakdown voltage. Figure 18 shows the power and efficiency plots at both of the designed frequencies. The design achieves a peak efficiency of 91.5% at 15.5 MHz. Finally, it is ready to test the design with the DBD loads as shown in Figure 19. The function generator is programmed to output a series of 12.4 MHz gate pulses followed by an idle period (setting gate to low), and then output a series of 15.5 MHz gate pulses followed by another idle period. The 12.4 MHz and 15.5 MHz operations are both set to 1000 cycles with a burst frequency of 100 Hz. At 12.4 MHz, plasma is generated on the left electrode (Figure 20(a)), and at 15.5 MHz, plasma is generated on the right electrode (Figure 20(b)). Figure 21 shows the measured output voltages and input power when the designed power amplifier drives the DBD loads. At both frequencies, the plasma starts at an input voltage of around 60 V and an input power of around 100 W. After the breakdown, the measured voltage across the plasma load remains at about 720 V<sub>rms</sub> regardless of the input power. Since the plasma load is variable and difficult to measure precisely, the measurements of the output power and efficiency when directly driving the DBD loads are neglected.



**TABLE 3.** Comparison of This Work With High-Frequency Wideband Power Amplifiers in the Literature

	This Work	[20]	[25]	[19]	[26]
Topology	Class E	PPT Class $\Phi_2$	Push-Pull Class E	Push-Pull Class E	Class E
Frequency [MHz]	12.4-15.5	12.56-18.06	8-12	1.8-128	20.86-27.12
Output Power [W]	600	300	2.9	200	58.6
Efficiency	91.5%	85-93%	80-88%	70-90%	N/A
Technique	Reactance Compensation	Reactance Compensation	Loading Network Tuning	Tunable Capacitor	Switched Capacitor

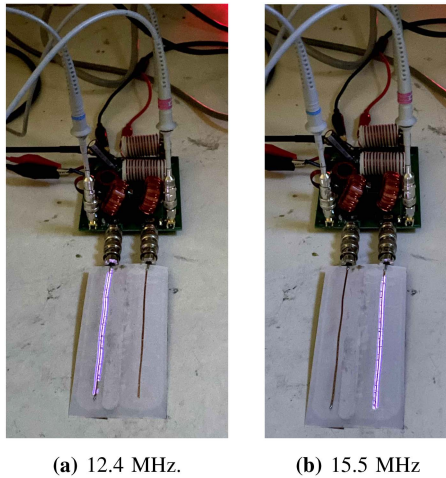


**FIGURE 20.** Photos of plasma generated (a) on the left electrode at 12.4 MHz, and (b) on the right electrode at 15.5 MHz with an input voltage of 150 V.

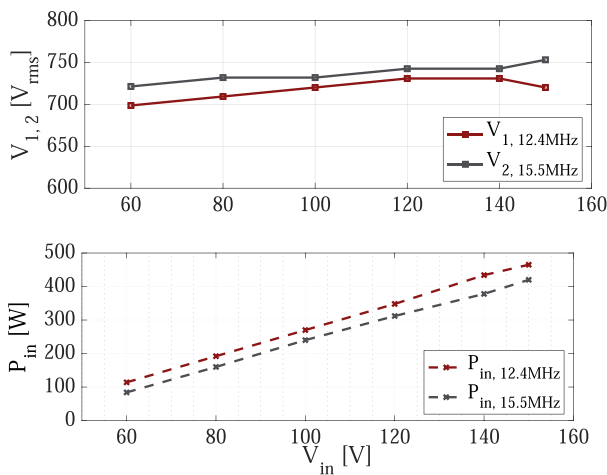


**FIGURE 21.** Measured output voltages and input power across the plasma load when the designed power amplifier drives the DBD loads.

Table 3 compares this design with the other high-frequency wideband power amplifiers in the literature. By using the reactance compensation technique, the design presented in this work does not require any additional switches, which simplifies the control and reduces cost. The design is able to maintain its high efficiency at two distinct frequencies,

12.4 MHz and 15.5 MHz, with an output power of 600 W. In addition to bandwidth extension, the frequency selection network also allows the designed power amplifier to deliver power to multiple loads selectively, which is an additional feature to all of the previous work in this table.

**V. CONCLUSION**

As an alternative for the Haber Bosch process, the plasma-assisted nitrogen fixation using the dielectric barrier discharge is able to achieve much cleaner and decentralized fertilizer production. This paper presents a frequency-selective Class E power amplifier that is able to drive DBD plasma loads sequentially at MHz frequencies by using the reactance compensation and frequency-selective resonant networks. The designed power amplifier is able to output 600 W at frequencies of 12.4 MHz and 15.5 MHz with a peak efficiency of 91.5%.

**ACKNOWLEDGMENT**

The authors would like to thank Stanford Woods Institute for the Environment for supporting this project.

**REFERENCES**

- [1] U.S. Geological Survey “Mineral commodity summaries,” 2021. [Online]. Available: <https://doi.org/10.3133/mcs2021>
- [2] C. Smith, A. K. Hill, and L. Torrente-Murciano, “Current and future role of Haber–Bosch ammonia in a carbon-free energy landscape,” *Energy Environ. Sci.*, vol. 13, pp. 331–344, 2020.
- [3] L. K. Boerner, “Industrial ammonia production emits more CO<sub>2</sub> than any other chemical-making reaction. Chemists want to change that,” *Chem. Eng. News*, vol. 97, no. 24, pp. 1–9, 2019.
- [4] C. Zamfirescu and I. Dincer, “Using ammonia as a sustainable fuel,” *J. Power Sources*, vol. 185, no. 1, pp. 459–465, 2008.
- [5] P. Lamichhane et al., “Low-temperature plasma-assisted nitrogen fixation for corn plant growth and development,” *Int. J. Mol. Sci.*, vol. 22, no. 10, 2021, Art. no. 5360.
- [6] H. Chen, D. Yuan, A. Wu, X. Lin, and X. Li, “Review of low-temperature plasma nitrogen fixation technology,” *Waste Disposal Sustain. Energy*, vol. 3, pp. 201–217, 2021.
- [7] C. Sze, B. Wang, J. Xu, J. Rivas-Davila, and M. A. Cappelli, “Plasma-fixed nitrogen as fertilizer for turf grass,” *RSC Adv.*, vol. 11, pp. 37886–37895, 2021.
- [8] S. Portugal, S. Roy, and J. Lin, “Functional relationship between material property, applied frequency and ozone generation for surface dielectric barrier discharges in atmospheric air,” *Sci. Rep.*, vol. 7, pp. 1–11, 2017.
- [9] J. P. Dedrick, “Radio-frequency surface discharges and their application to active flow control,” Ph.D. dissertation, Res. Sch. Phys. Eng., Australian Nat. Univ., Canberra, ACT, Australia, 2013.
- [10] N. Kumar, C. Prakash, A. Grebennikov, and A. Mediano, “High-efficiency broadband parallel-circuit class E RF power amplifier with reactance-compensation technique,” *IEEE Trans. Microw. Theory Techn.*, vol. 56, no. 3, pp. 604–612, Mar. 2008.

- [11] Y. Han, O. Leitermann, D. A. Jackson, J. M. Rivas, and D. J. Perreault, "Resistance compression networks for radio-frequency power conversion," *IEEE Trans. Power Electron.*, vol. 22, no. 1, pp. 41–53, Jan. 2007.
- [12] A. S. Jurkov, A. Radomski, and D. J. Perreault, "Tunable matching networks based on phase-switched impedance modulation," *IEEE Trans. Power Electron.*, vol. 35, no. 10, pp. 10150–10167, Oct. 2020.
- [13] L. Roslaniec, A. S. Jurkov, A. Al Bastami, and D. J. Perreault, "Design of single-switch inverters for variable resistance/load modulation operation," *IEEE Trans. Power Electron.*, vol. 30, no. 6, pp. 3200–3214, Jun. 2015.
- [14] J. Dedrick, R. W. Boswell, P. Audier, H. Rabat, D. Hong, and C. Charles, "Plasma propagation of a 13.56 MHz asymmetric surface barrier discharge in atmospheric pressure air," *J. Phys. D: Appl. Phys.*, vol. 44, no. 20, 2011, Art. no. 205202.
- [15] "RO4000 series high frequency circuit materials, rogers corporation," 2018. [Online]. Available: <https://www.rogerscorp.com/advanced-electronics-solutions/ro4000-series-laminates>
- [16] H. H. Wu, G. A. Covic, J. T. Boys, and D. J. Robertson, "A series-tuned inductive-power-transfer pickup with a controllable ac-voltage output," *IEEE Trans. Power Electron.*, vol. 26, no. 1, pp. 98–109, Jan. 2011.
- [17] Y.-J. Kim, D. Ha, W. J. Chappell, and P. P. Irazoqui, "Selective wireless power transfer for smart power distribution in a miniature-sized multiple-receiver system," *IEEE Trans. Ind. Electron.*, vol. 63, no. 3, pp. 1853–1862, Mar. 2016.
- [18] A. Al Bastami, A. Jurkov, D. Otten, D. T. Nguyen, A. Radomski, and D. J. Perreault, "A 1.5kW radio-frequency tunable matching network based on phase-switched impedance modulation," *IEEE Open J. Power Electron.*, vol. 1, pp. 124–138, 2020.
- [19] F. H. Raab, "Broadband class-E power amplifier for HF and VHF," in *Proc. IEEE MTT-S Int. Microw. Symp. Dig.*, 2006, pp. 902–905.
- [20] Z. Tong, L. Gu, and J. Rivas-Davila, "Wideband PPT class  $\Phi_2$  inverter using phase-switched impedance modulation and reactance compensation," *IEEE Trans. Ind. Electron.*, vol. 69, no. 6, pp. 5724–5734, Jun. 2021.
- [21] J. Zhou, K. A. Morris, G. T. Watkins, and K. Yamaguchi, "Improved reactance-compensation technique for the design of wideband suboptimum class-E power amplifiers," *IEEE Trans. Microw. Theory Techn.*, vol. 63, no. 9, pp. 2793–2801, Sep. 2015.
- [22] J. Xu, Z. Tong, and J. Rivas-Davila, "1 kW MHz wideband class E power amplifier," in *Proc. IEEE 22nd Workshop Control Modelling Power Electron.*, 2021, pp. 1–6.
- [23] S. C. Cripps, *Advanced Techniques in RF Power Amplifier Design*. Boston, MA, USA: Artech House, 2002.
- [24] H. Wang, C. Sideris, and A. Hajimiri, "A CMOS broadband power amplifier with a transformer-based high-order output matching network," *IEEE J. Solid-State Circuits*, vol. 45, no. 12, pp. 2709–2722, Dec. 2010.
- [25] R. A. Beltran, "Broadband outphasing transmitter using class-E power amplifiers," in *Proc. IEEE MTT-S Int. Microw. Symp.*, 2019, pp. 67–70.
- [26] A. S. Jurkov, "Techniques for efficient radio frequency power conversion," Ph.D. dissertation, Dept Elect. Eng. Comput. Sci., Massachusetts Inst. Technol., Cambridge, MA, USA, 2019.